Journal of Materials Chemistry C

Accepted Manuscript

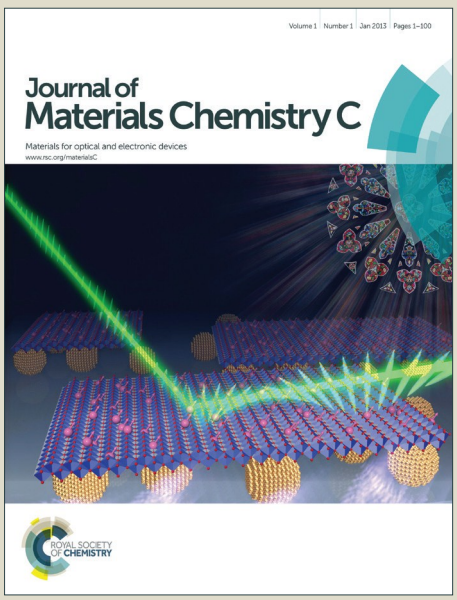

ROYAL SOCIETY OF CHEMISTRY

www.rsc.org/materialsC

Highly sensitive photodetectors using ZnTe/ZnO core/shell nanowire field effect transistors with a tunable core/shell ratio

Mehrdad Shaygan [1*], Keivan Davami [2,3], Bo Jin[4], Thomas Gemming[5], Jeong-soo Lee[4], M. Meyyappan[6]

[1]Advanced Microelectronic Center Aachen (AMICA), AMO GmbH, Otto-Blumenthal straße 25, 52074 Aachen, Germany

[2]Department of Mechanical Engineering and Applied Mechanics, University of Pennsylvania, Philadelphia, PA 19104, USA

[3]Department of Mechanical Engineering, Widener University, One University Place, Chester, PA 19013, USA

[4]Department of Electrical Engineering, Pohang University of Science and Technology, Pohang, South Korea

[5]IFW Dresden, P.O. Box 270116, D-01171 Dresden, Germany

[6]NASA Ames Research Center, Moffett Field, CA 94035, USA

Abstract

Fabrication and characterization of a field effect transistor using radial core/shell structure based on ZnTe nanowire is reported here. The electronic and photoconductive performance of the devices is successfully controlled by tuning the shell to core ratios in the integrated devices. The ZnO shell around the ZnTe nanowire has a significant effect on the optical properties of the transistor, and the photo-to-dark current ratio, responsivity and photoconductive gain are greatly enhanced to 199, 196 and 8.12×10^4 % respectively for the 17.5% shell/core ratio. The ability to control the core/shell ratio presented here is promising in device design for optoelectronic applications for covering a wide range of wavelengths.

Keywords:

Core/shell nanostructure, 1-D nanostructure-based device, nanowire field effect transistor, photodetector.

1. Introduction

Semiconductor nanowires exhibit interesting electrical, magnetic, optical, and thermoelectric properties compared to their bulk counterparts due to several favorable factors such as the density of electronic states, diameter-dependent bandgap and high surface to volume ratio [1,2]. Nanowire field effect transistors (NWFETs) using various semiconductor nanowires have received much attention in recent years due to the superior crystallinity and size-confined transport properties of the nanowires [1]. Semiconductor nanowires in heterostructure configurations result in an increase in the carrier mobility due to the reduced scattering and impressive optoelectronic features [3, 4]. Qian et al. [5] showed that core/multishell structure of a nanowire with a tunable bandgap responded to variable emission from 365 to 600 nm with a high quantum efficiency attributed to the improved properties of the optical cavity. The shell layer as a conformal coating around the core decreases the surface states as non-radiative carrier traps by passivation of the surface. It can also control the surface reactivity and the surface states while improving the interaction with the surrounding medium without changing the optical and electrical properties of the core structure [3,6,7].

Various techniques have been reported for the growth of core/shell nanowires such as chemical vapor deposition (CVD) [6] and solution-based techniques [8,9] for a range of applications including lithium ion batteries [10], multistate memory [11], high efficiency diodes [5], photodetectors [3], photovoltaic cells [8,12], and theremoelectric devices [13]. In all growth techniques, the fabrication steps needed after the formation of the core/shell structure introduce some technical difficulties such as missing the precise alignment for the device components, achieving uniform doping profile etc., all of which affect the device performance. Here, we report a novel and efficient technique to fabricate a core/shell nanowire FET with high yield and improved device performance and sensitivity through controlling the length and width of the conducting channel. We have chosen ZnTe for the core as a direct band gap (2.26 eV) group II-

VI semiconductor suitable for various optoelectronic devices [14-17]. The formation of native oxide around ZnTe in the form of ZnO when exposed to ambient air helps to create the shell layer [18] but additional control on the thickness can be obtained through controlled annealing. Zinc oxide, a well-known II-VI compound semiconductor with a wide band gap (3.37 eV), is a potential candidate for a wide range of applications [1].

In this study, we first synthesized ZnTe/ZnO core/shell nanowires and then investigated the relation between the growth conditions and the crystallinity of the nanowire by scanning transmission electron microscopy (STEM), electron energy loss spectroscopy (EELS) and X-ray dispersive spectroscopy. Based on the gained knowledge, we then produced the desired core/shell structure on the fabricated NWFET, characterized the electrical properties of the transistor followed by an evaluation of the photoresponse characteristics of the ZnTe/ZnO core/shell NWFETs.

2. Experimental Work

2.1 Core/shell structure synthesis

The ZnTe nanowires were grown on silicon substrates covered with a 3 nm gold layer via the vapor-liquid-solid technique, as described earlier [18]. In order to study the effect of different oxidation variants on the ZnO shell thickness, transmission electron microscopy (TEM) imaging in both bright and dark field modes (BF, STEM-HAADF) was performed using a Tecnai F30 (FEI) scanning transmission electron microscope (STEM) operated at 300 kV equipped with electron energy loss spectrometer (EELS) and energy dispersive X-ray spectrometer (EDX). The ZnTe nanowires were dispersed in ethanol using an ultrasonic technique and a few droplets of the dispersion were deposited on a copper grid with a holey carbon film. The covered TEM grids with the ZnTe NWs were placed inside the furnace under vacuum and kept at room temperature

first for one hour to purge oxygen completely from the furnace tube. We investigated the effect of different parameters on the oxidation of ZnTe including temperature (200, 250, 300, 350 and 400 ^{o}C), time (0.5, 2, 4, 8 and 16 hours) and Ar/O_2 concentration (ratios of 4/1, 2.5/2.5, 1/4 and 0/5). For the first two sets of experiments studying the time and temperature effects on shell/core ratio, the nanowires were annealed under air and ambient pressure. To study the role of oxygen concentration, the temperature and time were set at 250 ^{o}C and four hours, respectively.

2.2 Device fabrication

The ZnTe nanowires were removed from the substrate by scratching followed by dispersion in ethanol solution. A *p*-type Si with a 300 nm oxide layer acting as the back gate was used as the substrate. To disperse the nanowires on the target substrate, droplet dispersion coating was used to obtain a uniform and high yield of nanowire distribution on the substrate. Then, a layer of AZ5214E resist was formed on the middle section of the nanowire semiconductor structure by employing a specific hard mask patterning and conventional lithographical techniques. Wet chemical etching employing a HF solution (5%) for 15 seconds was followed by rinsing with DI water to remove the residues of HF. The HF-based solution removed the native oxide of ZnTe at the contact areas of the FET selectively while the covered resist protected the middle section. Metal layers of chromium/gold (30 nm / 180 nm) as electrodes were deposited over the entire substrate and the remaining portions of the metal layer were removed together with the patterned photoresist layer by conventional lift-off techniques to form the final structure of the FET. For the formation of a uniform longitudinal core/shell structure on the fabricated device, the designed thermal annealing for obtaining the targeted shell/core ratio was done. Moreover, the thermal annealing treatment helped greatly to reduce the contact resistance in the source and drain contacts [19].

The electrical characteristics of the devices were measured using an Agilant 4156C semiconductor parameter analyzer with a probe station. For the photoresponse characteristics, a light source of a 500 W-tunable Hg (Xe) lamp and a monochromator (Comerstone 130) were used to generate monochromatic light from 300 to 900 nm.

3. Results and Discussion

3.1 Effect of various parameters on the formed oxide shell

Figure 1a depicts an as-grown ZnTe nanowire with a 3 nm ZnO as native oxide. The existence of this 3 nm oxide shell in all the nanowires could be due to exposure to the ambient environment right after the synthesis or oxygen leakage during growth [18]. The EDX analysis of this nanowire (not shown here) confirmed the chemical composition as Zn, Te and oxygen. Any further annealing helps to increase the oxide thickness above this 3 nm. Annealing treatment at 250 ^{o}C for four hours led to an oxide shell of about 5 nm thickness uniformly around the nanowire (Fig.1b). The shell/core ratio is about 10 % while the oxide thickness could be varied between 5.4 – 5.8 nm for core diameters of 50 to 56 nm.

In order to study the chemical composition of ZnTe/ZnO core/shell nanowire, STEM investigation was conducted on the ZnTe nanowire annealed at 250 ^{o}C for four hours as shown in Fig. 2. It shows a high-angle annular dark field-STEM image of 85 nm diameter nanowire. A set of 41 EEL spectra was acquired across the nanowire marked with the red line in the STEM dark-field image (section *a*) with a spatial step size of about 1.5 nm. The examples of Te and oxygen-K are shown in panels *c* and *d* depicting the distribution of elements across the ZnTe nanowire after the annealing treatment. The oxygen seems to have concentrated more on the surface of the nanowire while Te mostly in the center of the nanowire. The observed phenomenon of the oxidation on the surface of the nanowire as a strictly thermal process involves the diffusion of the

Zn atoms to the surface followed by the formation of ZnO due to reaction with oxygen in air. The observed Te is confined to the core of the nanowire in ZnTe and there is no radial variation of Te. In contrast to the ZnTe/ZnO sequence found in our nanowires, ZnTe/Te/ZnO sequence has been observed previously in the oxidation of ZnTe thin films [20]. In the thin film case, a clear orientation of crystals together with some small regions of metal Zn was seen and in parallel, formed Te as a metal phase had a clear crystal orientation between ZnTe and ZnO layers [20]. In contrast, in our core/shell nanowire, a crystalline structure of ZnTe and amorphous of ZnO is observed clearly in the HRTEM images. Finally, the probability of ZnO formation instead of TeO_2 is attributed to the higher stability of ZnO than TeO_2 considering their different heats of formation (323.9 kJ/mol and 347.8 kJ/mol for TeO_2 and ZnO respectively) [21].

Annealing of a ZnTe nanowire at 300 ^oC results in the formation of the oxide shell with a 7.37 % shell/core ratio. TEM images (not shown here) of a 86.2 nm diameter ZnTe nanowire annealed at 350 ^oC showed an oxide thickness of about 8.3 nm leading to 9.6 % shell/core ratio, while 400 ^oC annealing led to the formation of an oxide shell of about 11 nm and shell/core ratio of 11%. Annealing temperatures of 400 ^oC and above could cause a partial melting in the nanowire, based on the size dependent behavior of melting temperature in ZnTe nanowires [18].

Another key parameter in forming the shell around the nanowire during the intentional oxidation process is time, and an annealing time of 0.5 and 2 hours was not able to make a significant change on the formed oxide similar to what was obtained by annealing at 300 ^oC. As seen in Fig. 1 (panels *c* and *d*), the thickness of the oxide shell increased significantly for annealing times of 8 and 16 hours resulting in a higher shell/core ratio up to 17.5. Varying the annealing time by keeping the annealing temperature far from the melting point of ZnTe nanowire could form thicker ZnO shell. Besides the temperature and annealing time, a mixture of gases including Ar and O_2 was used to evaluate the impact on the oxide shell thickness.

Increasing the percentage of oxygen in the gas flow during the annealing treatment resulted in some change in the formed shell with 5.1, 5.8, 6.7 and 7.6 nm for Ar and O_2 mixtures with ratios of 4/1, 2.5/2.5, 1/4 and 0/5, respectively.

3.2 Electrical and photoconductive characterization of the core/shell NWFET

A schematic view of the fabricated ZnTe/ZnO core/shell NWFET is shown in Fig. 3a and a top-view SEM image of a single ZnTe/ZnO NWFET annealed at 250 ^{o}C for 8 hours is depicted in Fig 3b. The nanowire diameter is 84.6 nm with a ZnO thickness of 12 nm, and the channel length (L) of this FET is 4.25 μm. Figure 3c shows the drain current (I_{ds}) versus drain–source voltage (V_{ds}) measured at gate voltages swept from -10 V to 10 V to characterize the electrical properties. The nonlinear behavior of the *I-V* curves is due to the Schottky barrier formed on the metal-semiconductor interfaces [19]. The drain current versus gate voltage measured at a constant V_{ds} =1 V is shown in panel *d* where the conductance of the nanowire increases with the gate voltage (negative polarity). The threshold gate voltage (V_{th}) and the transconductance (g_m) can be extrapolated as -6 V and 18.2 pS, respectively. The calculated carrier mobility (μ_h) and nanowire capacitance [22] for the ZnTe nanowire in the back-gated FETs are 9.5×10^{-3} cm^2 V^{-1} s^{-1} and 3.5×10^{-1} pF, respectively. The mobility value is higher than the reported values for ZnTe nanoribbons [23] and nanowires [24] but lower compared to bulk and thin films of ZnTe [25]. The electrical performance in Fig. 3 for the core/shell device is not much different from that of a bare device (not shown here). Here, the contact areas of the nanowires in the core/shell device are completely etched by HF solution, and the ZnTe nanowire without any oxide is in contact with the metal electrodes. Any slight improvement in performance could be attributed to the effect of annealing in improving the contact resistance [19]. There could be other advantages over bare devices as in the case of core/shell silicon NWFETs which have been shown to exhibit much

improved hysteresis due to the oxide shell acting as the passivation layer for the channel to limit the adsorption of gases [26].

The devices with different shell/core ratios were illuminated with vertical monochromatic light and the corresponding *I-V* curves were recorded (Fig. 4) to study the performance of the NWFET as a photodetector. The wavelength of the light was changed from 700 nm to 300 nm and the detectable wavelength for ZnTe and ZnO are 500 nm and 350 nm, respectively, considering their bandgap [27]. Figure 4a shows the typical current versus voltage relation under dark and illuminated conditions for the NWFET with a shell/core ratio of 10 when the light intensity was kept constant at 550 μWcm^{-2}. The Schottky contact between the NW and Cr/Au contacts led to the nonlinear behavior of the *I-V* curves. The fabricated NWPD was able to detect the visible light and the measured photocurrent decreases with an increase in the wavelength similar to previous reports [28] . The photocurrent arises mainly from the generation of electron-hole pairs by photons with a higher energy than the bandgap. The dynamic range of the photodetector is determined by the bandgap of the material as the conductivity of the photodetector can be modulated by the photogenerated carriers [29]. Figures 4b and c depict the photodetection performance of the NWPD for the shell/core ratios of 12.3 and 17.5 %, respectively. The sensitivity of the core/shell photodetector to the UV region increases significantly as the thickness of the ZnO shell is increased. The interface of ZnTe and ZnO, as in other core/shell structures such as In_2O_3/ZnO [30], contains a high density of surface states due to the lattice mismatch between the layers with no coherent atomic arrangement [31]. These traps at the heterointerface play a key role in the photoconducting behavior of the device via occupancy of the photogenerated carriers. Thermal annealing treatments could also induce defect states at the heterointerface [32]. Different optical transition processes could be produced into the bandgap of the material by means of these induced defect states. The photon absorption in the UV-Vis region

increases which, together with the main and sub-band gap transition, will enhance the optical absorption [33].

For ZnO nanostructures, a hole accumulation layer near the surface of the nanowire was reported as the reason for enhanced photocoductance. Under dark conditions, oxygen adsorption from air on the surface of ZnO forms a depletion layer near the surface ($O_2\,(g) + e^- \rightarrow O_2^-\,(ad)$). The incident light with a higher energy than the bandgap of ZnO generates electron-hole pairs where the holes migrate to the surface by surface recombination ($O_2^-(ad) + h^+ \rightarrow O_2\,(g)$), discharge the adsorbed oxygen ions and lead to photodesorption of oxygen on atoms [27]. The induced surface band bending by the electron depletion layer is able to separate the photogenerated electron-hole pairs resulting in suppressed photocarrier recombination and significantly prolonged carrier lifetime. Moreover, the photo-generated holes participate in oxygen desorption on the surface leading to the releasing back of the captured free electrons and further increase of free carrier concentration. These mechanisms are responsible for the high photoconductive gain of single crystalline ZnO nanowires as an *n*-type semiconductor [34]; similarly the same mechanism could be proposed for a *p*-type ZnO shell in our core/shell structure. The morphology of ZnO and the type of observed *I-V* curves determine the *p*-type nature of ZnO since the formation of nano-p-n junctions is inevitable in the case of *n*-type ZnO [35].

The photodetector performance of the fabricated NWFETs with different shell/core ratios is shown in Fig. 5a for various light wavelengths. Upon UV light illumination (300 nm), the photo (I_{ph})-to-dark current (I_{dark}) ratio I_{ph}/I_{dark} reached 1.95 for a device with a shell/core ratio of 10%. In the case of 12.3%, the I_{ph}/I_{dark} ratio increased to 2.62 while this value rose significantly to 199 for a shell/core ratio of 17.5 %. The photo-generated electrons in the ZnO shell layer

recombine with induced surface traps at the ZnTe/ZnO interface and a number of holes would be available for the photocurrent conduction [33].

The importance of core/shell semiconductor nanowires in photodetection can also be recognized by the spectral photoresponse measurements including photoresponsivity and photoconductive gain as shown Fig. 5b and c. The responsivity and photoconductive gain were calculated by $R_\lambda = I_{ph}/(P_{opt}S)$ and $G = (I_{ph}/q)/(P_{opt}S/h\upsilon)$ respectively, where I_{ph} is the photocurrent, P is the incident light intensity, S is the effective illuminated area, q is the electronic charge, h is the Planck`s constant, and ν is the frequency of incident light [27]. The illuminated surface of the device was estimated from the SEM images of the devices. The responsivity and photoconductive gain with 300 nm UV illumination for a shell/core ratio of 10% are 1.9 (A/W) and 8×10^2 % respectively; increasing the ratio to 12.3% enhanced these metrics by an order of magnitude to 15.2 (A/W) and 6×10^3%, respectively. A shell/core ratio of 17.5% boosted the performance significantly to 196 A/W and 8.12×10^4 %. The photoresponse in the regime higher than 400 nm is governed by radial Schottky junctions and band-band absorption due to the presence of interfacial defects [36]. The observed performance for the 17.5% case is better than several other material systems including ZnS, ZnSe, Sb_2Se_3, In_2Se_3 and others as summarized in ref. [37, 38].

4. Conclusion

We have presented a simple technique for making core/shell structures to construct nanowire field effect transistors. The desired shell/core ratio was achieved by controlling different parameters including temperature, time and Ar/O_2 content. The electrical characterization of ZnTe/ZnO core/shell nanowire field effect transistors verifies *p*-type behavior

with higher carrier mobility than previous reports in the literature. They respond to a wide range of incident light from visible to UV while the thickness of the shell layer has a significant effect on the final photoresponse. Increasing the shell/core ratios of the device from 10 % to 17.5 % improves the I_{ph}/I_{dark}, responsivity, and photoconductive gain from 1.95, 1.9 (A/W), 8×10^2 % to 199, 196 (A/W) and 8.12×10^4 %, respectively. Overall, these results highlight the potential of core/shell structure based nanowire FETs for optoelectronic applications.

References

1. M. Meyyappan and M. K. Sunkara, *Inorganic Nanowires: Application, Properties and Characterization*. 2010, *CRC Press*, Boca Raton, FL .
2. K. W. Kolasinski, *Current Opinion in Solid State and Materials Science*., 2006, **10**, 182-191.
3. X. Dai, S. Zhang, Z. Wang, G. Adamo, H. Liu, Y. Huang, C. Couteau and C. Soci, *Nano Lett.*, 2014, **14**, 2688-2693.
4. B. Hua, J. Motohisa, Y. Kobayashi, S. Hara and T. Fukui, *Nano Lett.,* 2009, **9**, 112-116.
5. F. Qian, S. Gradecak, Y. Li, C.-Y. Wen and C. M. Lieber, *Nano Lett.*, 2005, **5**, 2287-2291.
6. N. O. V. Plank, H. J. Snaith, C. Ducati, J. S. Bendall, L. Schmidt-Mende and M. E. Welland**,** *Nanotechnol.,* 2008, **19**, 465603.
7. L. Schmidt-Mende, and J. L. MacManus-Driscoll, *Mater. Today*., 2007, **10**, 40-48.
8. J. Tang, Z. Huo, S. Brittman, H. Gao and P. Yang, *Nat. Nanotechnol.*, 2011, **6**, 568-572.
9. A. Dong, F. Wang, T. L. Daulton and W. E. Buhro, *Nano Lett.,* 2007, **7**, 1308-1313.
10. L. -F. Cui, R. Ruffo, C. K. Chan, H. Peng and Y. Cui, *Nano Lett.,* 2009, **9**, 491-495.
11. Y. Jung, S. -H. Lee, A. T. Jennings and R. Agarwal, *Nano Lett.*, 2008, **8**, 2056-2062.
12. J. A. Czaban, D. A. Thompson and R. R. LaPierre, *Nano Lett.*, 2009, **9**, 148-154.
13. G. Zhang, W. Wang and X. Li, *Adv. Mater.*, 2008, **20**, 3654-3656.
14. T. Tanaka, K. Saito, M. Nishio, Q. Guo and H. Ogawa, *Appl. Phys. Exp.*, 2009, **2**, 122101.
15. J. Schrier, D. O. Demchenko, L. -W. Wang and A. P. Alivisatos, *Nano Lett.*, 2007, **7**, 2377-2382.
16. Q. Wu, M. Litz and X. C. Zhang, *Appl. Phys. Lett.*, 1996, **68**, 2924-2926.
17. Z. Liu, G. Chen, B. Liang, G. Yu, H. Huang, D. Chen and G. Shen, *Optics Express*, 2013, **21**, 7799-7810.
18. M. Shaygan, T. Gemming, V. Bezugly, G. Cuniberti, J. -S. Lee and M. Meyyappan, *J. Phys. Chem. C.*, 2014, **118**, 15061-15067.
19. H. Faryabi, K. Davami, N. Kheirabi, M. Shaygan, J. -S. Lee and M. Meyyappan, *Chem. Phys. Lett.*, 2012, **543**, 117-120.
20. P. Lu and D. J. Smith, *Physica Status Solidi (a).*, 1988, **107**, 681-691.

21. O. Kubaschewski, E. L. L. Evans and C. B. Alcock, *Tables. Metallurgical Thermochemistry,* 1979 **1**.

22. O. Wunnicke, *Appl. Phys. Lett.*, 2006, **89**, 083102.

23. S. Li, Y. Jiang, D. Wu, L. Wang, H. Zhong, B. Wu, X. Lan, Y. Yu, Z. Wang and J. Jie, *J. Phys. Chem. C.* 2010, **114**, 7980-7985.

24. Y. L. Cao, Y. B. Tang, Y. Liu, Z. T. Liu, L. B. Luo, Z. B. He, J. S. Jie, R. Vellaisamy, W. J. Zhang and C. S. Lee, *Nanotechnol.*, 2009, **20**, 455702.

25. A. Barati, A. Klein and W. Jaegermann, *Thin Solid Films.*, 2009, **517**, 2149-2152.

26. T. Kawashima, T. Saitoh, K. Komori and M. Fujii, *Thin Solid Films.* 2009, **517**, 4520-4526.

27. M. Shaygan, M. Meyyappan and J. -S. Lee, *Nanowire Field Effect Transistors in Optoelectronics*, in *Nanowire Field Effect Transistors: Principles and Applications*. 2014, *Springer*, 187-224.

28. Z. Li, J. Salfi, C. De Souza, P. Sun, S. V. Nair and H. E. Ruda, *Appl. Phys. Lett.*, 2010, **97**, 063510.

29. T. Zhai, X. Fang, M. Liao, X. Xu, L. Li, B. Liu, Y. Koide, Y. Ma, J. Yao and Y. Bando, *ACS Nano.*, 2010, **4**, 1596-1602.

30. S. Park, H. Ko, S. Kim and C. Lee, *ACS Appl. Mater. Interface.*, 2014, **6**, 9595-9600.

31. F. Säuberlich and A. Klein, *Mat. Res. Symp. Proc*. 2003, **763**. Cambridge Univ Press.

32. S. W. Xue, X. T. Zu, W. L. Zhou, H. X. Deng, X. Xiang, L. Zhang and H. Deng, *J. Alloys Compounds.*, 2008, **448**, 21-26.

33. J. C. Dhar, A. Mondal, N. K. Singh, S. Chakrabartty, A. Bhattacharyya and K. K. Chattopadhyay, *J. Appl. Phys.*, 2013, **114**, 244310.

34. C. Soci, A. Zhang, B. Xiang, S. A. Dayeh, D. P. R. Aplin, J. Park, X. Y. Bao, Y. -H. Lo and D. Wang, *Nano Lett.*, 2007, **7**, 1003-1009.

35. Y. Lin, W. -J. Chen, J. Y. Lu, Y. H. Chang, C. -T. Liang, Y. F. Chen and J. -Y. Lu, *Nanoscale Res. Lett.*, 2012, **7**, 1-5.

36. C. -Y. Hsu, D. -H. Lien,S. -Y. Lu, C. -Y. Chen, C. -F. Kang, Y. -L. Chueh, W. -K. Hsu and J. -H. *ACS Nano.*, 2012, **6**, 6687-6692.

37. D. Kang, T. Rim, C. K. Baek, M. Meyyappan and J. -S. Lee, *Small,* 2014, **10**, 3795-3802.

38. M. Shaygan, K. Davami, N. Kheirabi, C. K. Baek, G. Cuniberti, M. Meyyappan, and J. -S. Lee, Phys. Chem. Chem. Phys. 2014, **16**, 22687-22693.

Figure captions

1: HRTEM images of a ZnTe nanowires, (a) without annealing treatment; (b-d) annealed at 250 ^{o}C for 4, 8 and 16 hours respectively.

2: (a) A high-angle annular dark field (HAADF)-STEM image of an 85 nm diameter ZnTe nanowire annealed at 250 ^{o}C for four hours. (b) The brightness profile of the HAADF-STEM image. Measured EELS: Te (c) and O K-edge (d) of the ZnTe nanowire along the red line shown in (a).

3: (a) Schematic view of the ZnTe/ZnO core/shell NW field effect transistor. (b) A top-view SEM image of a device annealed at 250 ^{o}C for 8 hours. The nanowire diameter is 84.6 nm with a ZnO thickness of 12 nm and the channel length is 4.25 μm. (c) I_{ds}-V_{ds} measured at gate voltages (V_g) varying from -10 V to 10 V. (d) drain current versus gate voltage curves obtained at a constant V_{ds} = 1 V.

4: I-V relation of the ZnTe/ZnO core-shell NW photodetector in dark and under illumination with various wavelengths of light for different shell/core ratios: (a) 10%, (b) 12.3% and (c) 17.5%.

5: Optical characteristics of the ZnTe/ZnO core/shell photodetectors with different shell/core ratios. (a) I_{ph}/I_{dark} ratio, (b) responsivity, and (c) photoconductive gain.

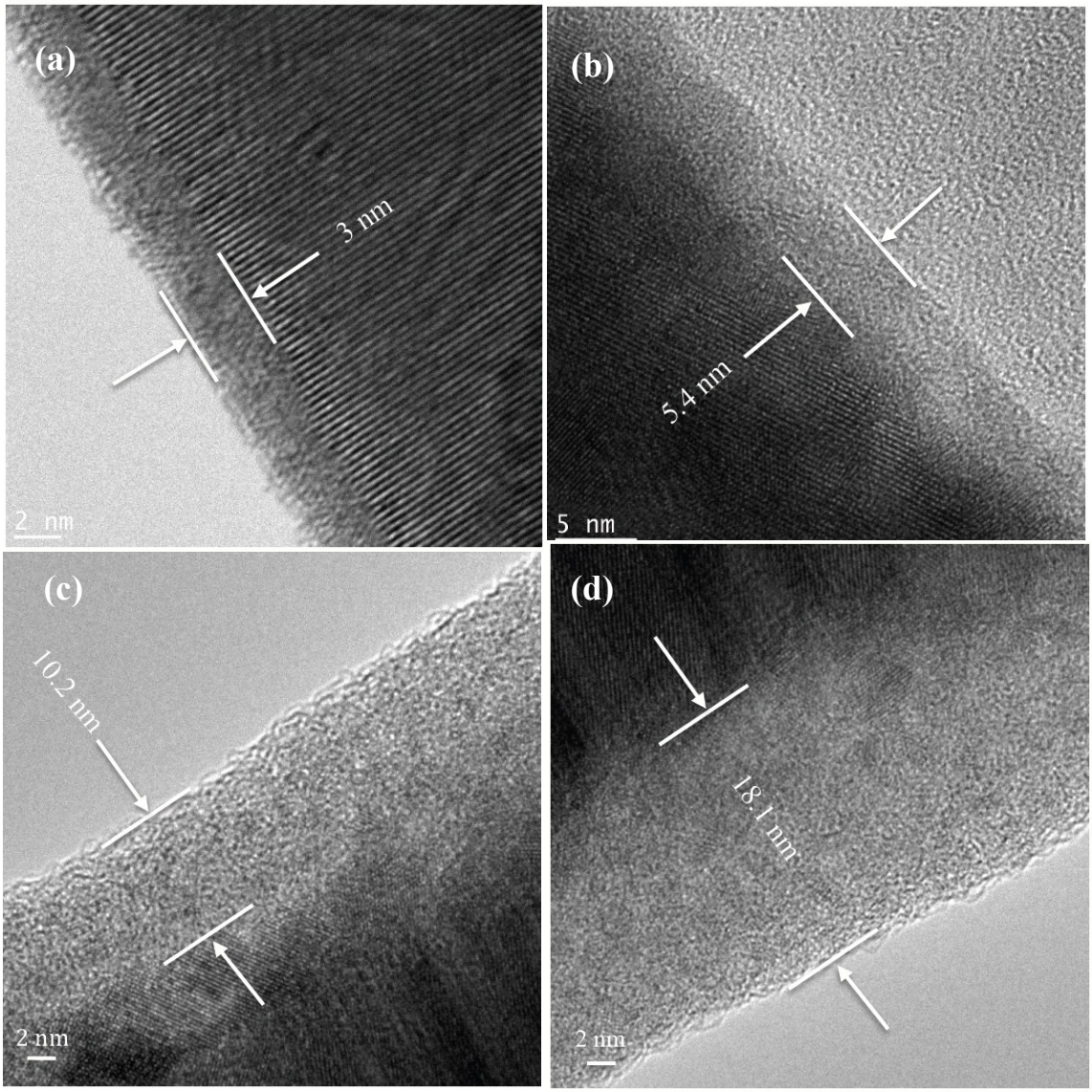

Figure 1

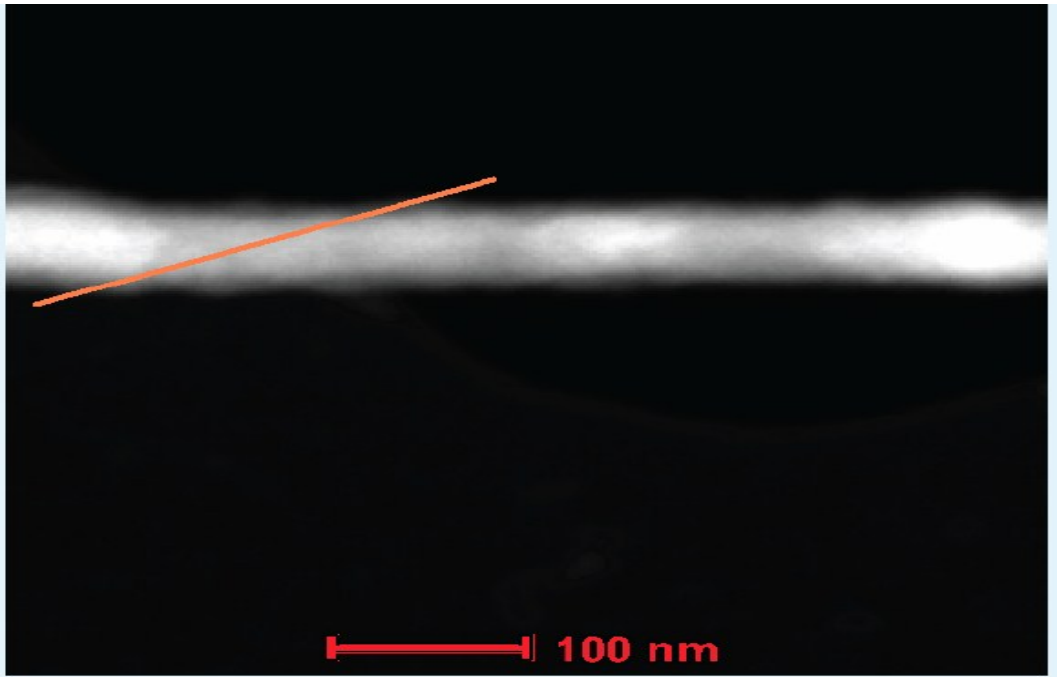

(a)

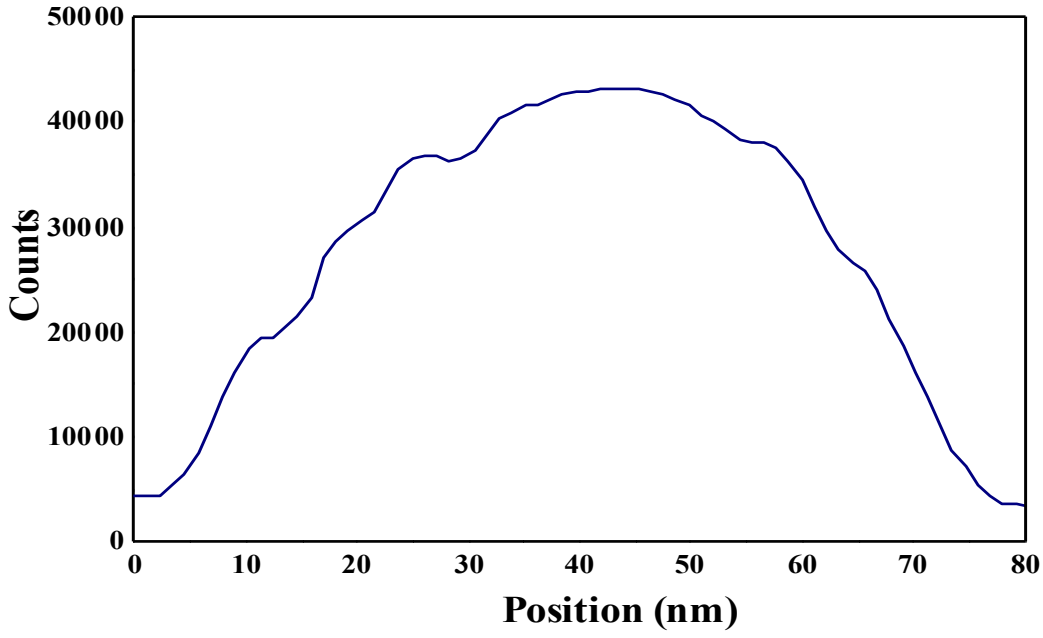

(b)

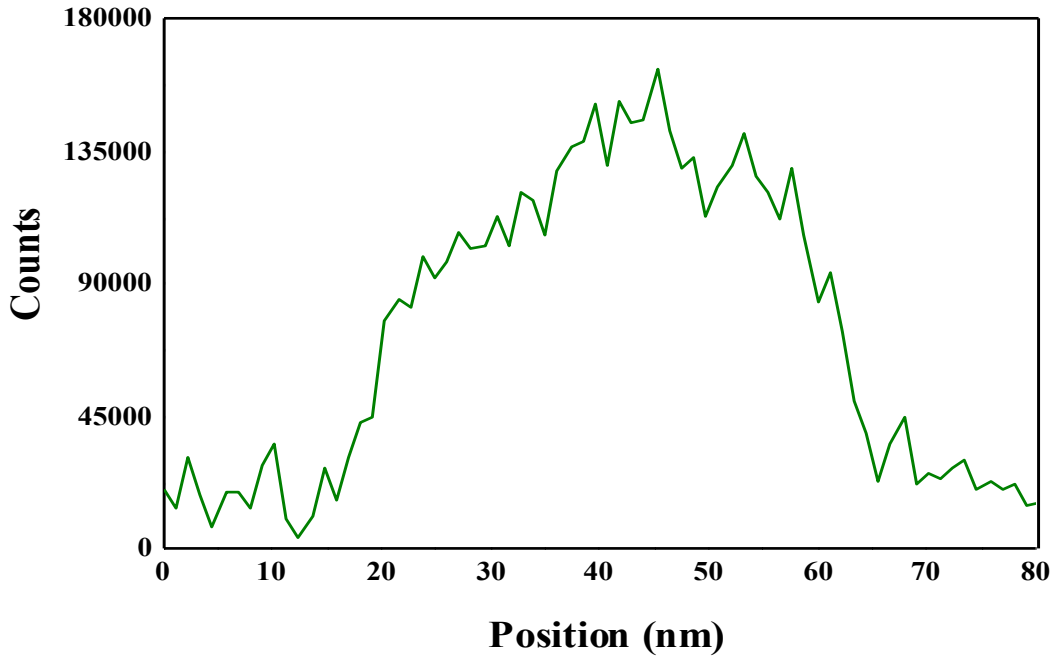

(c)

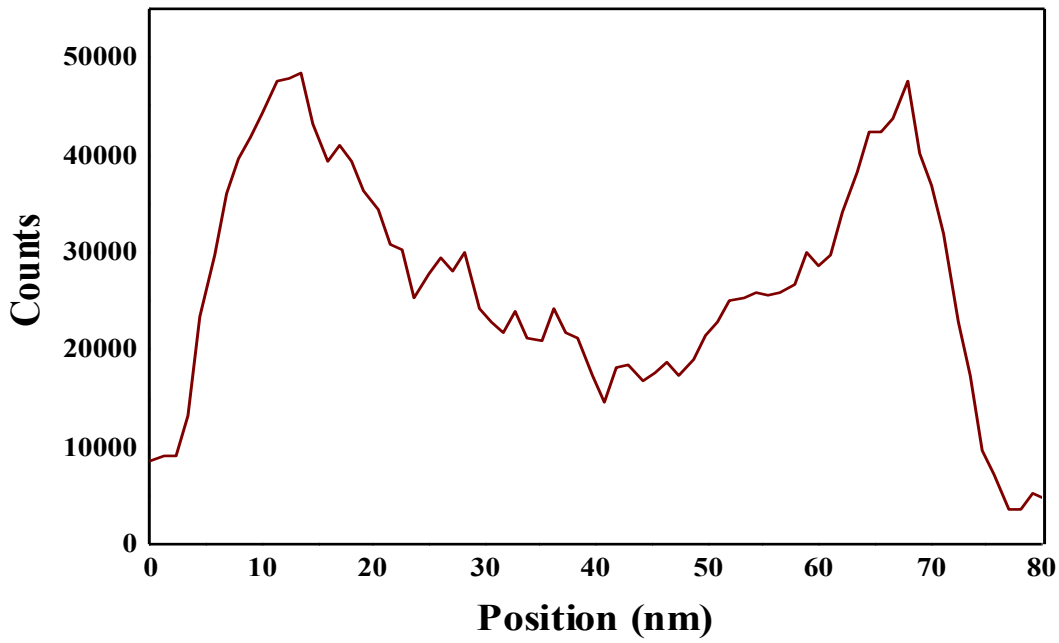

(d)

Figure 2

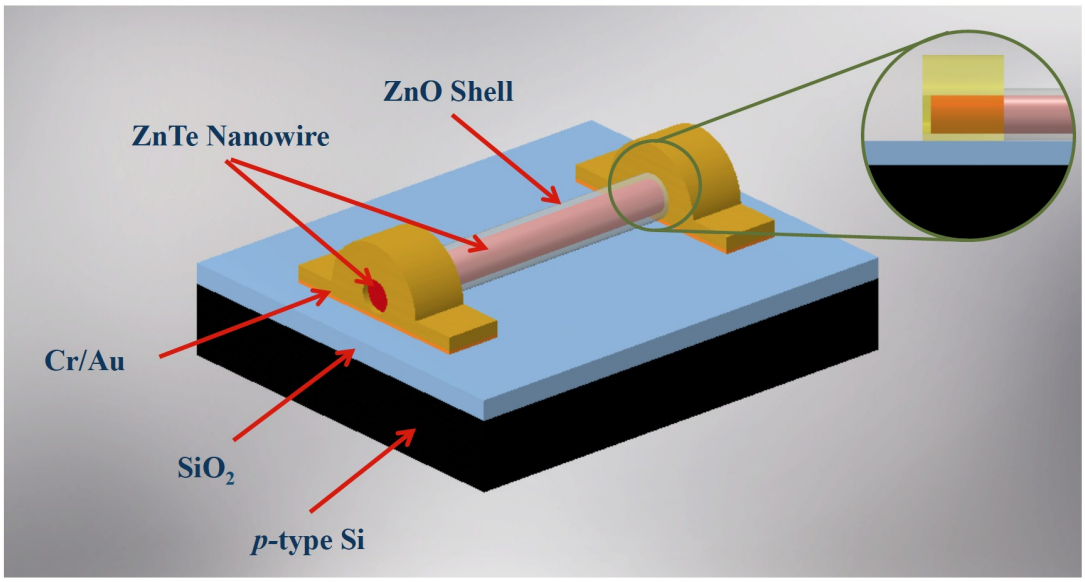

(a)

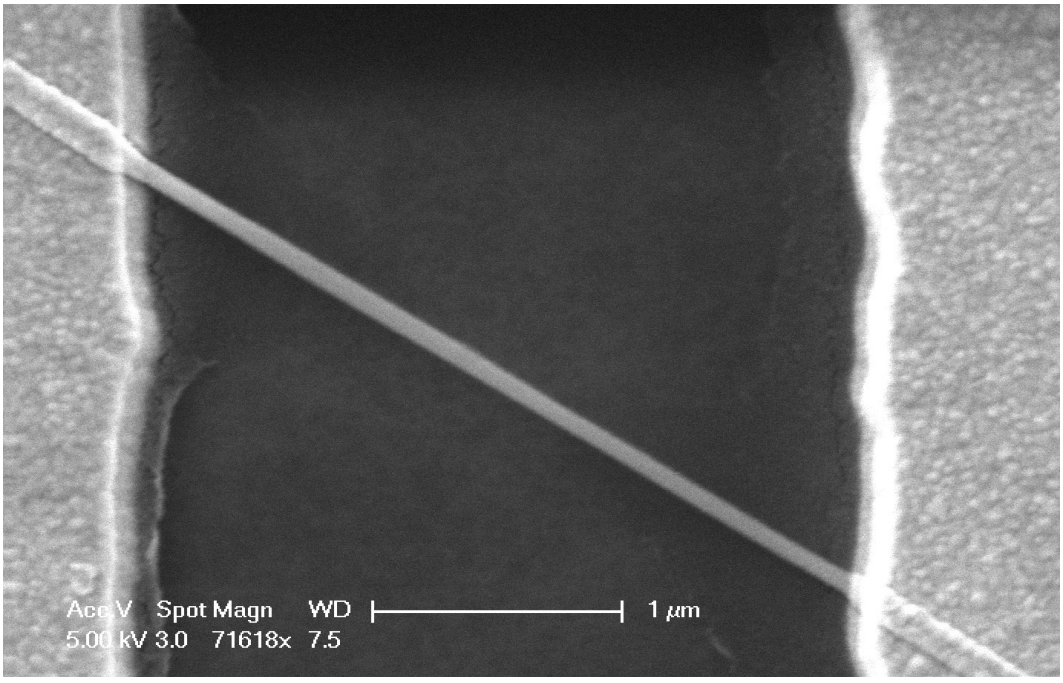

(b)

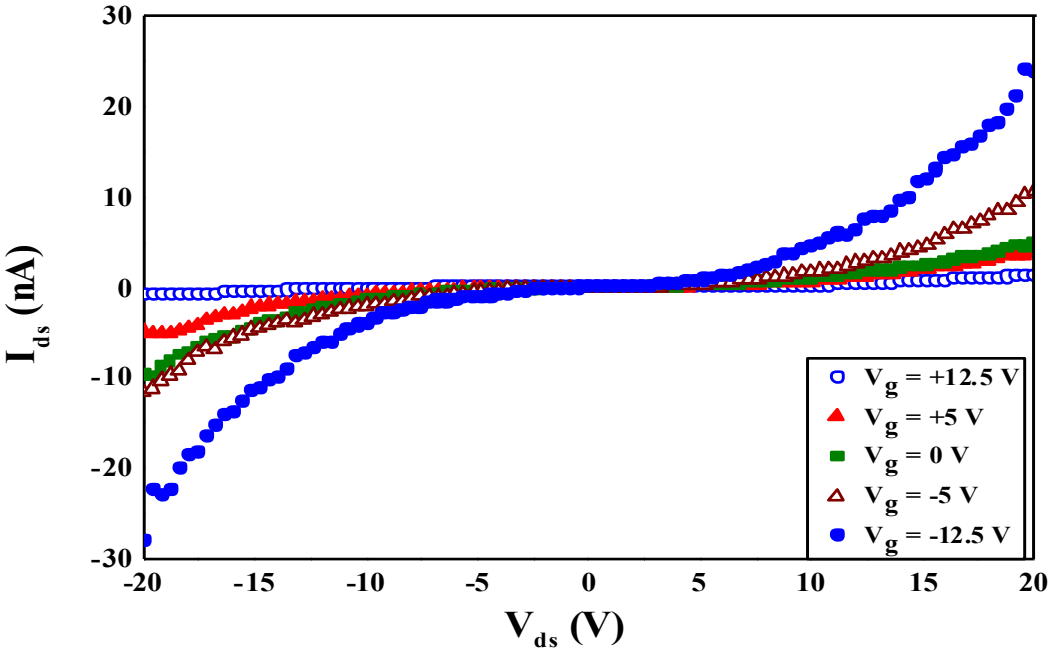

(c)

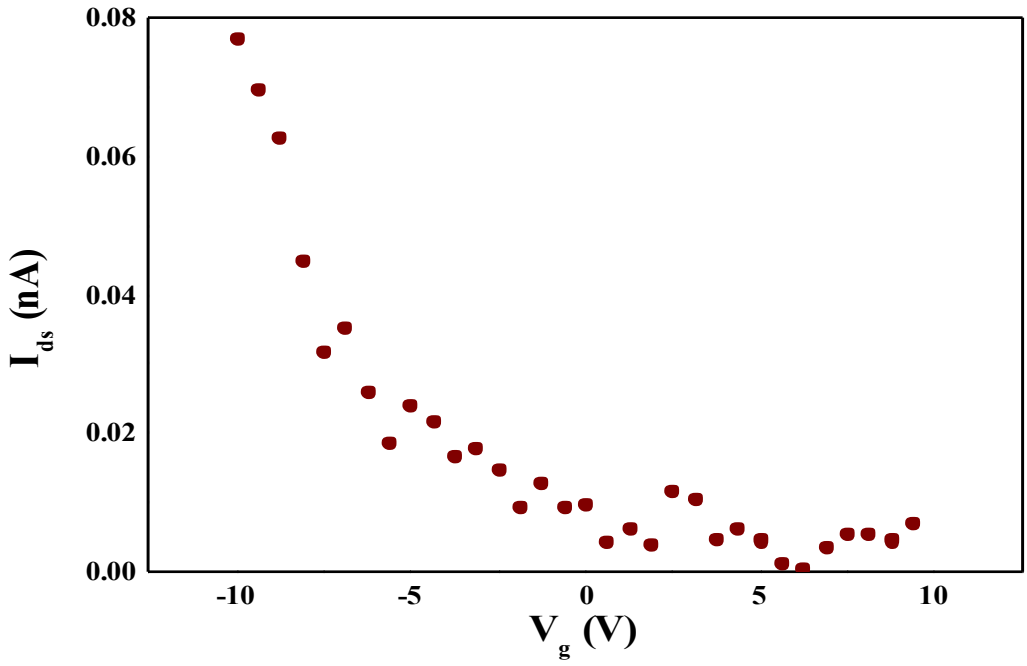

(d)

Figure 3

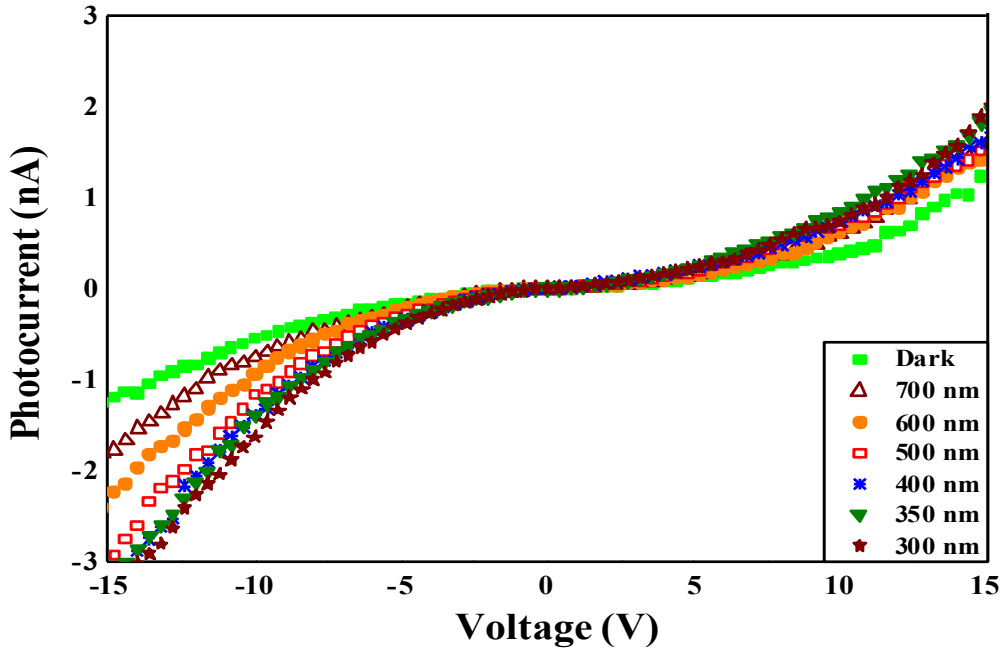

(a)

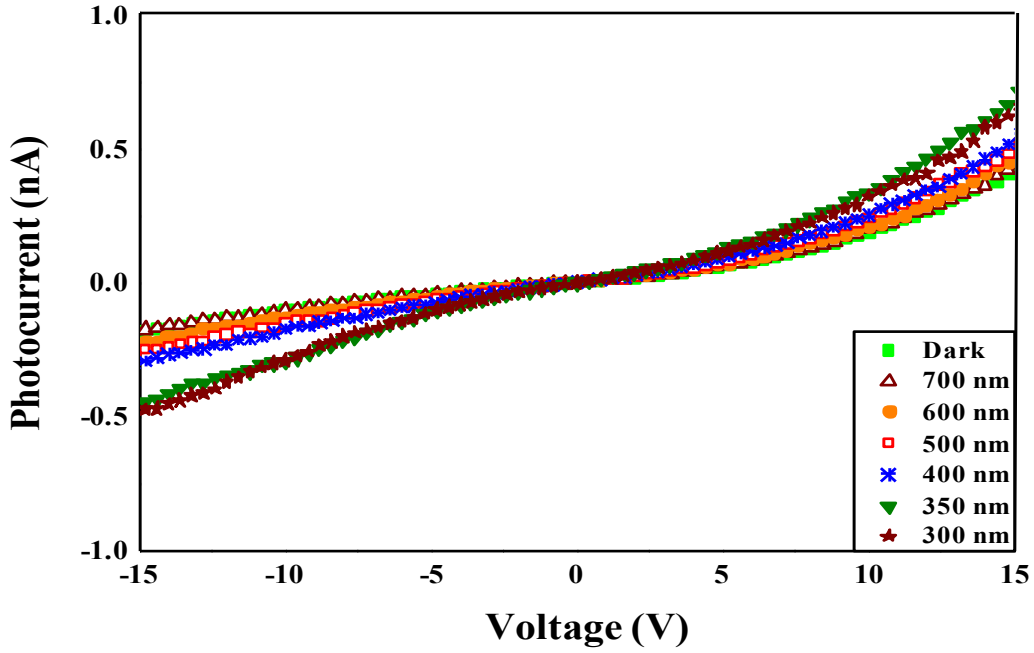

(b)

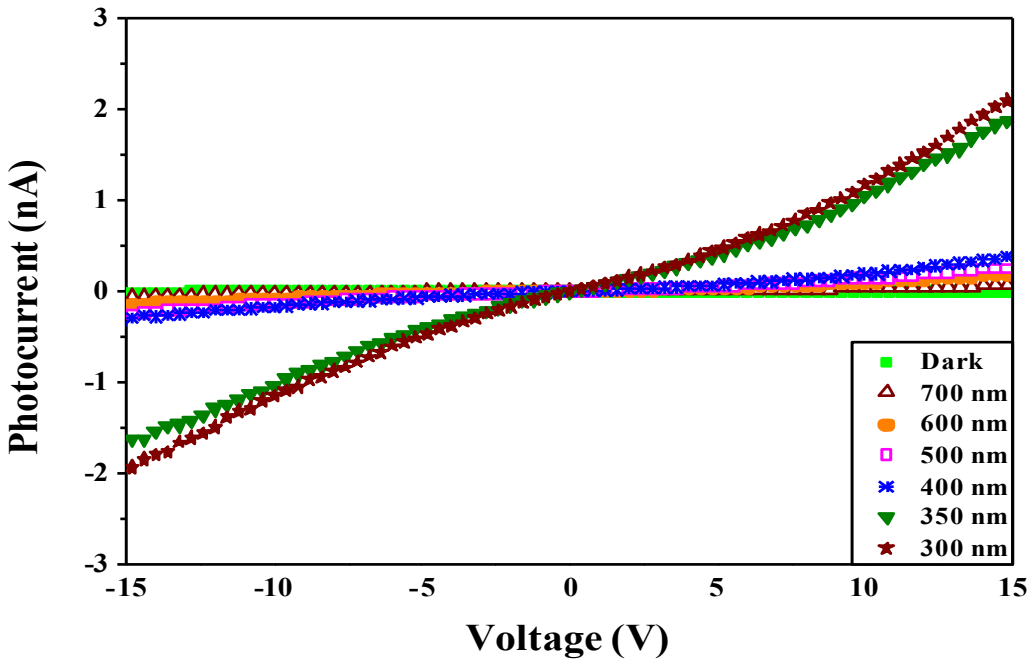

(c)

Figure 4

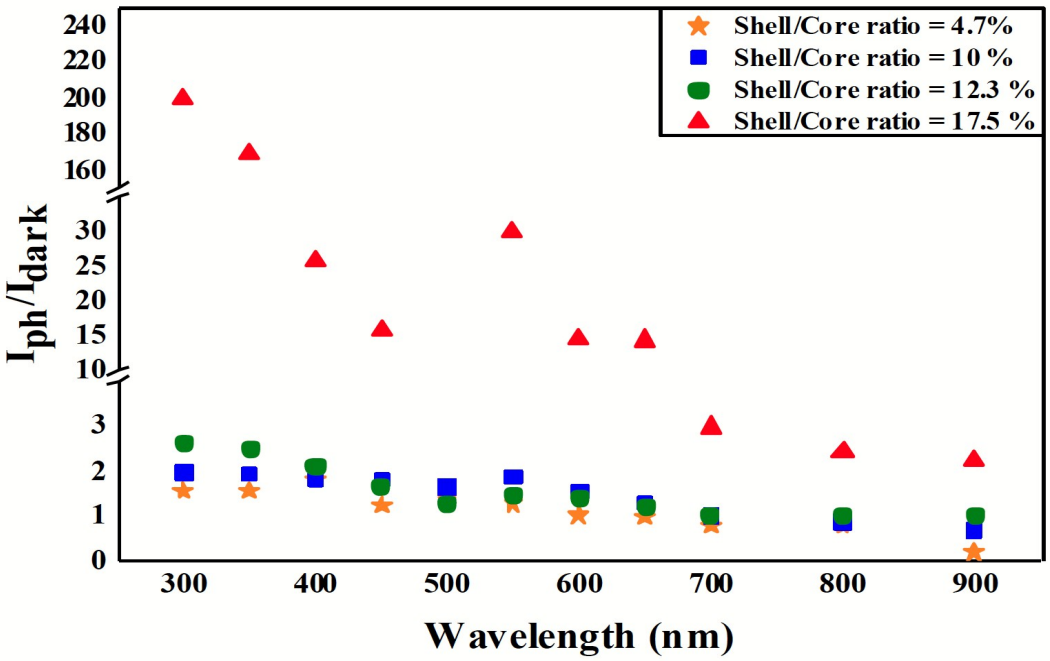

(a)

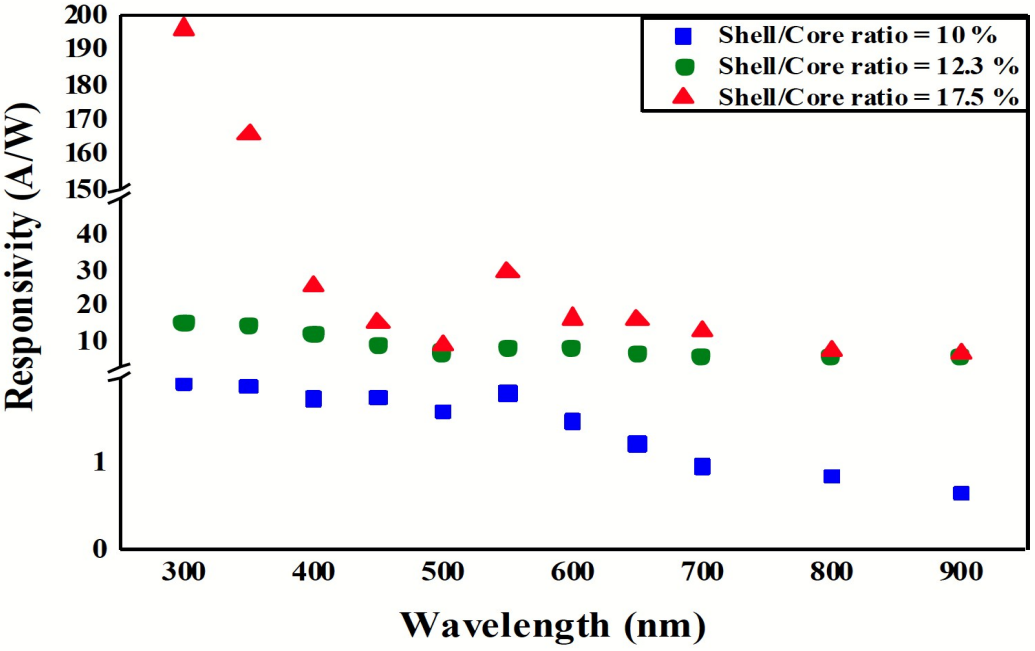

(b)

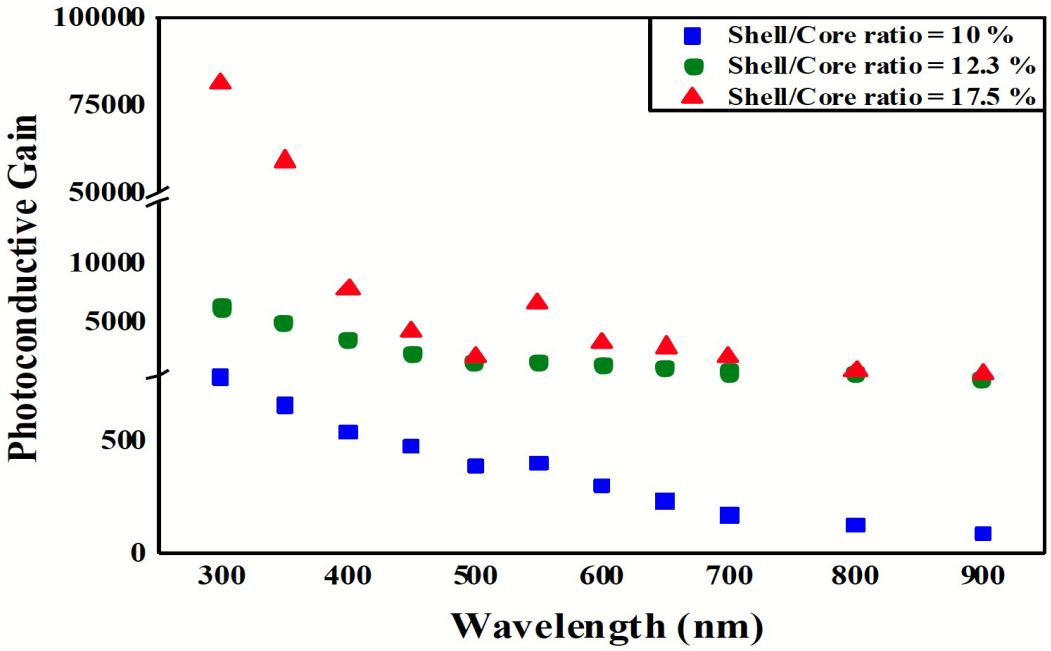

(c)

Figure 5

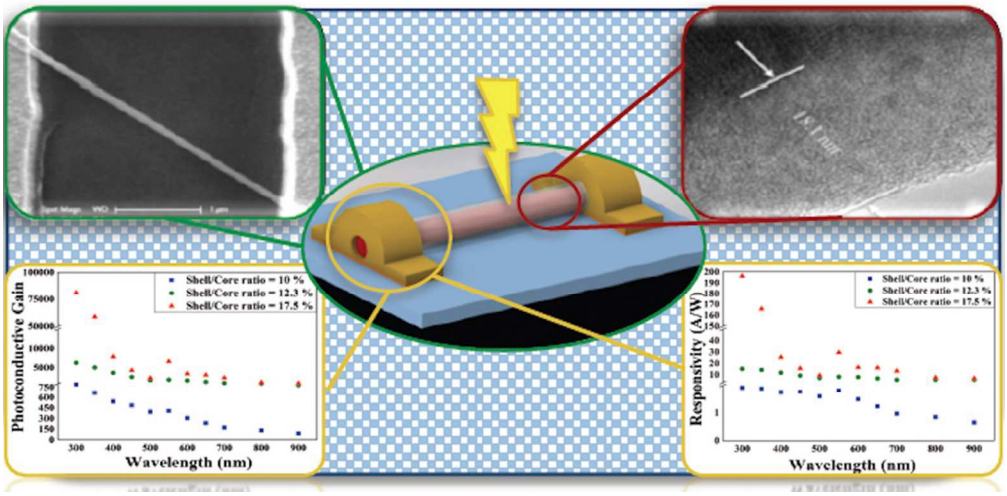

81x39mm (300 x 300 DPI)